Optical real-time monitoring of the laser molecular-beam epitaxial growth of perovskite oxide thin films by an oblique-incidence reflectance-difference technique

Fan Chen, Huibin Lu, Zhenghao Chen, Tong Zhao, and Guozhen Yang

Laboratory of Optical Physics, Institute of Physics, Center for Condensed Matter Physics, Chinese Academy of Sciences, P.O. Box 603, Beijing 100080, China

Received August 18, 2000; revised manuscript received January 17, 2001

We report the results of optical *in situ* monitoring of the epitaxial growth of perovskite oxide thin films by an oblique-incidence reflectance-difference (OIRD) technique. Optical oscillation that corresponds to the growth cycle of an interrupted growth mode (monolayer oscillation) is observed. The monolayer oscillation shows different behaviors for layer-by-layer, Stranski–Krastanow, and three-dimensional growth modes. Optical interference oscillation is observed. The dependencies of the real and the imaginary parts of the bulk film's refractive index on the OIRD signal are discussed and illustrated with a three-layer stack mode. Thin-film complex refractive-index and highly accurate thickness measurements can be obtained by fitting of the interference oscillation.

OCIS codes: 120.5700, 120.6660, 240.0310, 310.3840.

1. INTRODUCTION

The engineering of various high-speed semiconductor devices requires precise control of the thin-film thickness and the interfaces of the heterostructures. Real-time monitoring of thin-film growth can provide information on growth mode, film thickness, and thin-film quality and can be used for feedback control of thin-film growth. Reflection high-energy electron diffraction (RHEED) is the most widely used method for monitoring thin-film growth. It has been routinely used to control thin-film growth on an atomic scale in molecular-beam epitaxy[1,2] (MBE) and in laser MBE.[3,4] One can obtain various kinds of information about the growing surface from the RHEED pattern and the intensity oscillations. However, the application of RHEED is restricted to high-vacuum environments. Optical probe techniques are noninvasive and nondestructive and can be used in any transparent ambient. Reflectance-difference spectroscopy[5,6] (RDS), *p*-polarized reflectance spectroscopy,[7,8] and spectral ellipsometry[9] have been applied for a decade to monitor surface process and bulk-film properties. RDS measures the sample anisotropy along various crystal axes. RDS can provide real-time monitoring of chemical composition, electronic structure, and surface kinetics of III–V group growth. *p*-Polarized reflectance spectroscopy measures the reflectivity of the *p* polarization of the probe light at the Brewster angle. It provides information on growth rate and bulk optical properties of a film and on nucleation and overgrowth kinetics of heteroepitaxial growth under steady-state conditions.[7,8] However, most studies of these subjects were carried out on semiconductor materials. There are few reports of optical monitoring of the growth of oxides, except in Refs. 10 and 11, perhaps because of the structural and chemical complexity of the composition of perovskite oxides.

Previously,[10] the results of optical monitoring of $SrTiO_3$ homoepitaxy by an oblique-incidence reflectance difference (OIRD) technique were reported. The OIRD technique is a new type of reflectance-difference technique that measures the difference in reflectivity between *s* and *p* polarization. Unlike for the normal incidence of normal RDS, the probe beam of the OIRD is incident upon the substrate surface at an incident angle of approximately 83°–87°. The OIRD technique was used to study surface diffusion upon a metal surface[13,14] and has been demonstrated to be sensitive to a relative change in reflectivity of $\Delta R/R = 1 \times 10^{-5}$ and a change in coverage of $\Delta\theta = 0.02$.[13] The conventional RDS is applicable only to those materials that have surface anisotropy, but the OIRD measurement does not have such a limitation, as was proved previously[10] by monitoring of the interrupted growth of $SrTiO_3$ homoepitaxy. In this paper we report the results of optical monitoring during the epitaxial growth of perovskite oxides under conditions of laser MBE.[4] Optical oscillation corresponding to the growth cycle (monolayer oscillation) is observed for the heteroepitaxy of Nb-doped $SrTiO_3$ upon a $SrTiO_3$ substrate in an interrupted-growth mode.[4] The OIRD intensity shows a response that is consistent with RHEED intensity for good two-dimensional (2D) layer-by-layer growth. It is interesting that the monolayer oscillation becomes weak and noisy for the Stranski–Krastanow (SK) mode[15] [a mixture of 2D and three-dimensional (3D) island growth], and the monolayer oscillation vanishes for the 3D island-growth mode. Optical interference oscillation is observed for heteroepitaxy. The amplitude damp-

ing of the interference oscillation indicates optical adsorption by the bulk film. The damping speeds at different ambient-oxygen pressures permit monitoring of the relative oxygen content of as-grown thin films, as the optical absorption comes mainly from oxygen deficiency. Using a three-layer-stack, we show that the thin-film thickness and the complex refractive-index information can be obtained by fitting of the interference oscillation with Fresnel's equation for multilayers. The precision of the thickness monitoring can be at the unit-cell level because of the high signal–noise ratio of the OIRD measurement.

2. EXPERIMENTS

The measurements were performed in a laser MBE system[4] with a standard RHEED apparatus. The electron beam's incidence angle in RHEED is ~3° with respect to the surface plane, the so-called out-of-phase condition for RHEED measurement. A CCD camera is used to record the RHEED specular spot intensity. The optical setup of the OIRD is schematically illustrated in Fig. 1. The laser probe beam, with a wavelength of 632.8 nm from a 4-mW linearly polarized He–Ne laser, is initially *p* polarized. It is modulated by a photoelastic modulator before it is incident onto the substrate surface at a glancing angle of ~7° (the corresponding incident angle is ~83°). The *p*-polarization component bisects the two principal axes of the modulator, and this produces a phase shift between the two components along the principal axes at a frequency of $\Omega = 50\,\mathrm{kHz}$. The maximum phase is set at π, or 180°. The reflected beam is detected by a silicon photodiode, and the photocurrent goes into a Stanford Research Model 510 lock-in amplifier. The three parallel plates are adapted to adjust the relative intensity of the *s*- and *p*-polarized components to form a near-zero background. The monitored OIRD intensity can be given by[10,11]

$$I(2\Omega) = 1/2 J_2(\Phi) I_{\mathrm{inc}} \times [|r_p(\theta_{\mathrm{RDS}}) t_p(\theta_{\mathrm{tilt}})|^2 - |r_s(\theta_{\mathrm{RDS}}) t_s(\theta_{\mathrm{tilt}})|^2], \quad (1)$$

where $r_p(\theta_{\mathrm{RDS}})$ and $r_s(\theta_{\mathrm{RDS}})$ are the reflectance coefficients for *p*- and *s*-polarized light at incidence angle θ_{RDS} and $t_p(\theta_{\mathrm{tilt}})$ and $t_s(\theta_{\mathrm{tilt}})$ are the total transmission coefficients for *p*- and *s*-polarized light, respectively, through the fused-quartz plates at a tilt angle θ_{tilt}. $J_2(\Phi)$ is a Bessel function of the second kind. With proper adjustment of the three parallel plates, a near-zero background

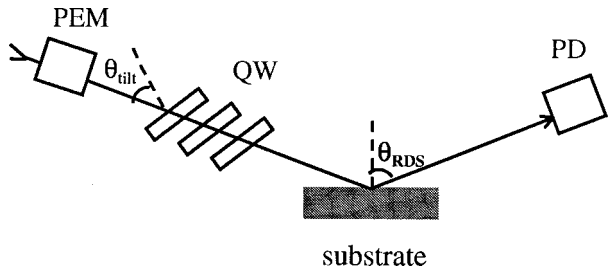

Fig. 1. Schematic of the optical setup for the OIRD measurement: PEM, photoelastic modulator; QW, fused-quartz parallel plate; PD, biased silicon photodiode.

intensity can be obtained when $|r_{p0}(\theta_{\mathrm{RDS}}) t_p(\theta_{\mathrm{tilt}})|^2 = |r_{s0}(\theta_{\mathrm{RDS}}) t_s(\theta_{\mathrm{tilt}})|^2$. We measured the relative OIRD intensity as given by

$$\frac{I}{I_{p0}} = \frac{\Delta R}{R_0} = \left(\left| \frac{r_p}{r_{p0}} \right|^2 - \left| \frac{r_s}{r_{s0}} \right|^2 \right), \quad (2)$$

where $I_{p0} = 1/2 J_2(\Phi) I_{\mathrm{inc}} |r_{p0}(\theta_{\mathrm{RDS}}) t_p(\theta_{\mathrm{tilt}})|^2$ is the initial reflected intensity of the *p*-polarization component.

The film growth is kept in a so-called interrupted-growth mode.[4,12] In the interrupted-growth mode the deposition is periodically interrupted after a certain amount of material has been deposited onto the substrate. Interrupted growth can successfully improve surface and interface smoothness and has proved to be an important method for studying surface kinetics.[12] We define deposition and its following interruption as a growth cycle. In our experiments, only one unit-cell layer was deposited in each growth cycle. The number of laser pulses needed for depositing one unit-cell layer was determined by the continuous RHEED intensity oscillation. Pure oxygen was introduced into the growth chamber as a source of ambient oxygen. Other growth conditions are the same as those reported previously.[10,11]

3. RESULTS AND DISCUSSION

Figure 2 shows the simultaneously measured OIRD response [Fig. 2(b)] and RHEED intensity oscillation [Fig. 2(a)] obtained for niobium-doped $SrTiO_3$ upon a $SrTiO_3(100)$ substrate in the interrupted-growth mode. The representations of deposition and interruption of the growth cycle are separated by dotted lines and are labeled. As shown in Fig. 2(a), the growth is interrupted at the top of the RHEED intensity oscillation, indicating that the growth proceeds in a good layer-by-layer growth mode. The OIRD intensity shows almost consistent response with the RHEED intensity except for an opposite direction. There is a similar maximum value of the OIRD signal before the end of each deposition compared with the RHEED intensity minimum value, which indicates surface roughening at a lower surface coverage than half-layer coverage, followed by smoothing with increasing coverage. The OIRD intensity recovers to its initial value when growth is interrupted, as does the RHEED intensity. The OIRD response in a good 2D layer-by-layer growth condition can be explained as being a result of periodically changed surface morphology with a four-layer-stack model.[11]

When the growth proceeds in a SK or a 3D island-growth mode, the OIRD intensity shows various responses, as in Fig. 3. Figure 3(d) shows the optical interference oscillation for the heteroepitaxy of $BaTiO_3$ upon a niobium-doped $SrTiO_3(100)$ substrate (the doping concentration is 1 mol %). Figures 3(a), 3(b), and 3(c) show detailed curves of the three positions as indicated by the arrows and the numerals 1, 2, and 3, respectively. The period of small oscillation corresponds to the growth cycle. The labels on and off indicate the start and interruption, respectively, of the deposition of each growth cycle. It is noticeable that the OIRD signal in Fig. 3(b) is

of opposite sign to that in Fig. 3(a). As indicated in Fig. 3(d), there is a so-called turning point[7,8] between points 1 and 2, as indicated by the arrows, after which the optical signal changes sign. The turning point was observed by Dietz and Bachmann[7] for *p*-polarized reflectance spectroscopy measurement of GaP grown upon a Si(100) substrate. The monolayer OIRD signal close to the turning point becomes weak and recovers when it is moved away from that point. We chose all three positions far from the turning point.

Because of lattice mismatch, the heteroepitaxial growth of $BaTiO_3$ upon a niobium-doped $SrTiO_3$(100) substrate proceeds in a SK growth mode at first. As shown in Fig. 3(a), the OIRD intensity goes downward during the deposition without a maximum value, which means that the surface continues to become rougher. When the deposition is interrupted, the surface smoothness begins to recover, as revealed by the recovery of the OIRD intensity. With increasing film thickness, the growth begins to be transformed from a SK growth mode into a 3D island-growth mode. As shown in Fig. 3(c), the monolayer OIRD signal vanishes, which can be explained as a result of the surface morphology's not having effectively recovered during the interruption. From Figs. 3(a)–3(c) we can see the transformation of the growth mode from a SK mode into a 3D island mode.

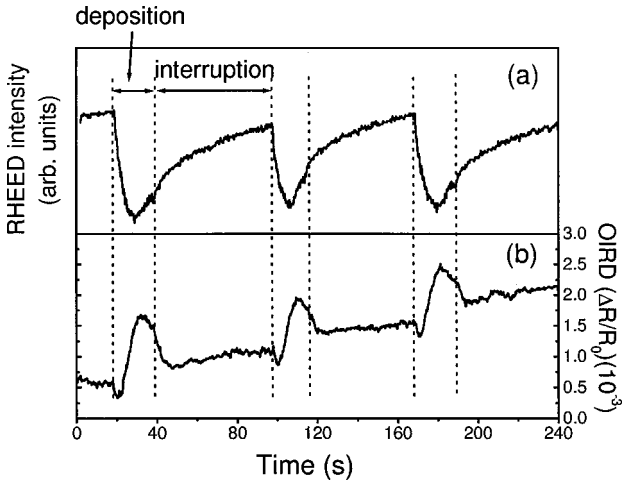

Fig. 2. (a) Consistent RHEED intensity oscillation and (b) OIRD relative intensity in a good 2D layer-by-layer growth mode of niobium-doped $SrTiO_3$ upon a $SrTiO_3$(100) substrate.

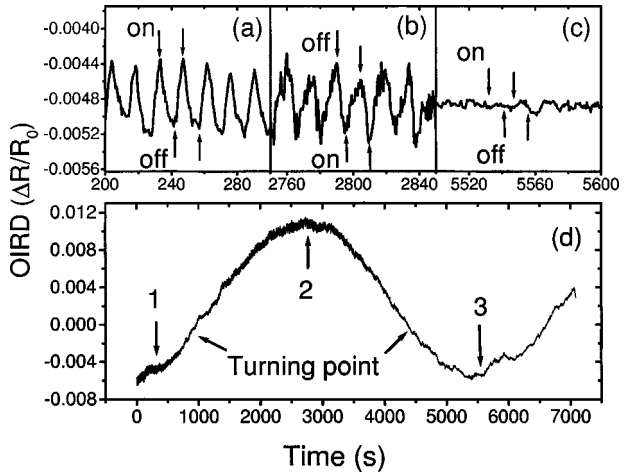

Fig. 3. (d) Interference oscillations and (a)–(c) monolayer oscillations obtained by OIRD during the heteroepitaxy of $BaTiO_3$ upon a $SrTiO_3$(100) substrate.

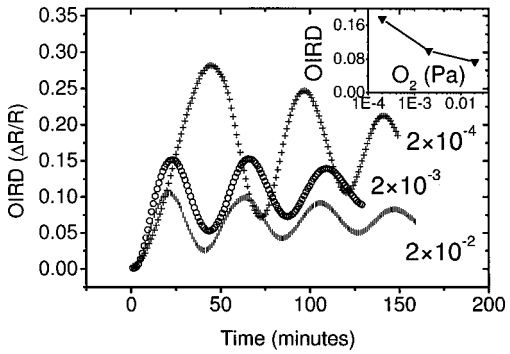

Fig. 4. OIRD interference oscillations of the heteroepitaxy niobium-doped $SrTiO_3$ upon a $SrTiO_3$(100) substrate under various ambient-oxygen pressures. The symbols graph the oxygen pressure (in pascals) as marked. Inset, the amplitude of the second oscillation as a function of growing oxygen pressure.

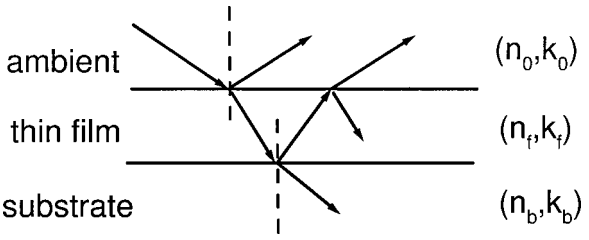

Fig. 5. Schematic illustration of the surface structure described by a three-layer stack model for heteroepitaxy in the OIRD measurement and the multiple reflections of the probe light beam from this stack.

Figure 4 shows the optical interference oscillations for the epitaxial growth of niobium-doped $SrTiO_3$ (the doping concentration is 10 mol. %) upon a $SrTiO_3$(100) substrate at several ambient-oxygen pressures. The three curves were obtained at oxygen pressures of 2×10^{-4}, 2×10^{-3}, and 2×10^{-2} Pa. The first property of the oscillations is that all the amplitudes damp with increasing thin-film thickness, indicating a nonzero imaginary part of the complex refractive index of the grown bulk film. Another is that the amplitude and the damping speed are much different for different ambient-oxygen pressures. As shown in the inset of Fig. 4, the amplitude of the oscillation (we chose the second cycle for comparison) decreases with increasing ambient-oxygen pressure.

Now we discuss the effect of the complex refractive index of the bulk film on the OIRD interference oscillations. The thin-film structure can be described as a three-layer stack (ambient–thin film–substrate), as shown in Fig. 5. When the probe laser beam is incident upon the substrate surface, multireflection occurs between the surface–thin-film interface and the thin film–substrate interface. A series of beams is reflected back to the ambient. The interference oscillation is an effect of interference of all the reflected beams. We used Fresnel's equations for a multilayer stack as described previously[16] to calculate the reflectivity of *s* and *p* polarization. By numbering the three-layer stack 0 for ambient, 1 for the thin film, and 2

for the substrate, we can denote the complex refractive index of the ambient, the thin film, and the substrate $\tilde{n}_0 = (n_0, k_0)$, $\tilde{n}_1 = (n_f, k_f)$, and $\tilde{n}_2 = (n_b, k_b)$, respectively.

The complex dielectric constant of each layer can be denoted $\tilde{\varepsilon}_k = (\tilde{n}_k)^2$ $(k = 0, 1, 2)$. The thickness of the film layer is denoted h. The reflection coefficient at the interface between layer k and layer $k + 1$ (from layer k to layer $k + 1$) is given by[11]

$$r^p_{k,k+1} = \frac{\varepsilon_{k+1}(\varepsilon_k - \varepsilon_0 \sin^2\varphi)^{1/2} - \varepsilon_k(\varepsilon_{k+1} - \varepsilon_0 \sin^2\varphi)^{1/2}}{\varepsilon_{k+1}(\varepsilon_k - \varepsilon_0 \sin^2\varphi)^{1/2} + \varepsilon_k(\varepsilon_{k+1} - \varepsilon_0 \sin^2\varphi)^{1/2}}, \tag{3}$$

$$r^s_{k,k+1} = \frac{(\varepsilon_k - \varepsilon_0 \sin^2\varphi)^{1/2} - (\varepsilon_{k+1} - \varepsilon_0 \sin^2\varphi)^{1/2}}{(\varepsilon_k - \varepsilon_0 \sin^2\varphi) + (\varepsilon_{k+1} - \varepsilon_0 \sin^2\varphi)^{1/2}} \quad (k \geq 0), \tag{4}$$

where φ is the angle of incidence from the ambient. Considering the interference effects of all the reflection beams from each layer as shown in Fig. 5, we can express the total reflectance coefficient in term of $r_{k,k+1}$ as[16]

$$r_p = \frac{r^p_{01} + r^p_{12}\exp(2i\phi)}{1 + r^p_{01}r^s_{12}\exp(2i\phi)}, \qquad r_s = \frac{r^s_{01} + r^s_{12}\exp(2i\phi)}{1 + r^s_{01}r^s_{12}\exp(2i\phi)}, \tag{5}$$

with phase factors $\phi = (2\pi/\lambda)(\varepsilon_1 - \varepsilon_0 \sin^2\varphi)^{1/2}$. $\lambda = 632.8$ nm is the wavelength of the probe light in vacuum. The reflection from the initial surface is a simple reflection from a single interface (ambient–substrate interface). The reflectance coefficients r_{p0} and r_{s0} are given by

$$r_{p0} = \frac{\varepsilon_2 \cos\varphi - \sqrt{\varepsilon_0}(\varepsilon_2 - \varepsilon_0 \sin^2\varphi)^{1/2}}{\varepsilon_2 \cos\varphi + \sqrt{\varepsilon_0}(\varepsilon_2 - \varepsilon_0 \sin^2\varphi)^{1/2}},$$

$$r_{s0} = \frac{\sqrt{\varepsilon_0}\cos\varphi - (\varepsilon_2 - \varepsilon_0 \sin^2\varphi)^{1/2}}{\sqrt{\varepsilon_0}\cos\varphi + (\varepsilon_2 - \varepsilon_0 \sin^2\varphi)^{1/2}}, \tag{6}$$

respectively.

The complex refractive index of the $SrTiO_3$ substrate at 632.8 nm is $\tilde{n}_2 = (n_b, k_b) = (2.38, 0.01)$, as determined by McKee *et al.*[17] The ambient is vacuum with a refractive index $\tilde{n}_0 = (1, 0)$. Then OIRD signals are calculated with Eqs. (2)–(6) as functions of thin-film thickness. Figure 6(a) shows the relationship among $R_p = |r_p|^2$, $R_s = |r_s|^2$, and the OIRD measurement with the thin-film complex refractive index $\tilde{n}_1 = (n_f, k_f) = (2.1, 0.01)$. The background R_{s0} and R_{p0} (of R_s and R_p, respectively) is successfully subtracted in the OIRD measurement. Figures 6(b) and 6(c) show the effects of the real part n_f and the imaginary part k_f on the OIRD signals. For a chosen substrate, in the case of $SrTiO_3$ $(n_b, k_b) = (2.38, 0.01)$, the relative OIRD signal increases with increasing $|n_f - n_b|$ when n_f ranges from 1.9 to 3.0. The signs of the interference oscillation for $n_f < n_b$ and $n_f > n_b$ are opposite. The interference oscillation period Δh decreases with increasing n_f, as given by $\Delta h = \lambda_0/2n_f \cos\theta_f$,[18] where θ_f is the refractive angle in the thin-film layer. As is shown in Fig. 6(c), the damping speed of the amplitude of the interference oscillations increases with higher k_f, indicating enhanced absorption of the probe light.

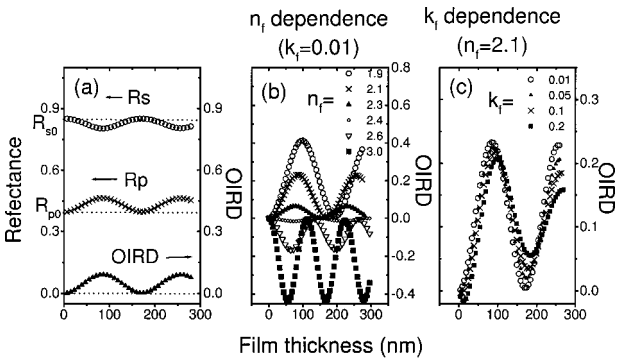

Fig. 6. Numerical simulation results of the OIRD measurement calculated from the three-layer stack with Fresnel's equations for multilayers: (a) reflectance of the s and p polarization and the relative OIRD signal as a function of thin-film thickness; (b) dependence of the OIRD signal on the real part of the complex refractive index of the thin-film layer; (c) dependence of the OIRD signal on the imaginary part of the complex refractive index of the thin-film layer.

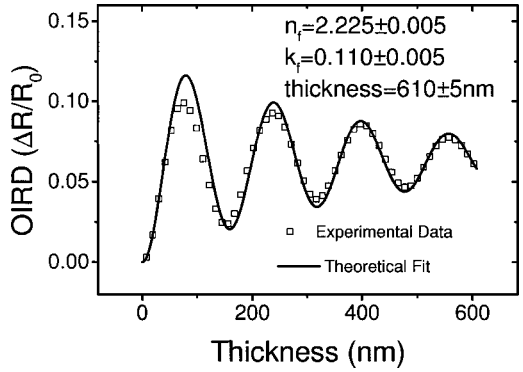

Fig. 7. Theoretical fit of the experimental data (niobium-doped $SrTiO_3$ upon $SrTiO_3$ at an oxygen pressure of 2×10^{-2} Pa). The fitted complex refractive index (n_f and k_f) and film thickness are shown.

According to the above discussion, one can calculate the thin-film thickness and the complex refractive index by fitting the experimental data. Figure 7 shows the fitting of the OIRD signal obtained at an oxygen pressure of 2×10^{-2} Pa, as shown in Fig. 4. The scatter graph (open squares) shows the experimental data (not all the data points are plotted). The solid curve is the fitted results. The thin-film complex refractive index and the thickness are obtained as $(2.225 \pm 0.005, 0.110 \pm 0.003)$ and 610 ± 5 nm, respectively. With the same method, the complex refractive indices of the thin films grown at oxygen pressures of 2×10^{-3} and 2×10^{-4} Pa are obtained as $(2.140 \pm 0.005, 0.116 \pm 0.003)$ and $(1.98 \pm 0.01, 0.125 \pm 0.003)$, respectively. The thicknesses are 490 ± 5 and 495 ± 5 nm, respectively. The fitting results show that the imaginary part of the refractive index is larger for lower-growth oxygen pressure. This study provides a method for real-time monitoring of the relative oxygen content of growing bulk film as well as of thin-film

thickness and growth rates. As for thickness monitoring, the precision can be at unit-cell level, as can be judged from the high signal–noise ratio shown in Fig. 2. The OIRD maximum intensity increase for the growth of one unit-cell layer can be obtained at the waist of the interference oscillations. A typical OIRD signal change for the growth of one unit-cell layer is 5×10^{-4} (Fig. 2). We can improve the fitting accuracy of the film-thickness measurement shown in Fig. 7 by simply increasing the data-acquisition speed.

4. CONCLUSIONS

In summary, we have reported the results of optical monitoring by the OIRD method of epitaxial growth of oxides under conditions of laser molecular-beam epitaxy. The growth mode can be revealed by the monolayer oscillation corresponding to the growth cycle of interrupted growth. The OIRD response is quite consistent with the RHEED intensity oscillation for 2D layer-by-layer growth. In the SK growth mode, the OIRD shows directly upward and downward behavior without maximum values before the end of the deposition. And the monolayer oscillation vanishes for 3D island growth. A three-layer stack model was used to represent the surface structure. The interference oscillation for heteroepitaxy can be well fitted with Fresnel's equations for multilayers. The complex refractive index and the thin-film thickness can be measured. The precision of the thickness monitoring can reach the unit-cell level because of the high signal-noise-ratio of the OIRD measurement. This study demonstrates that the OIRD is of potential use for monitoring growth mode, thickness, and complex refractive index of thin films.

ACKNOWLEDGMENT

This research was supported by a grant from the State Key program of China.

G.-Z. Yang's e-mail address is yanggz@aphy.iphy.ac.on.

REFERENCES

1. J. J. Harris, B. A. Joyce, and P. J. Dobson, "Oscillations in the surface structure of Sn-doped GaAs during growth by MBE," Surf. Sci. **103**, L90–L96 (1981).
2. J. J. Neave, B. A. Joyce, P. J. Dobson, and N. Norton, "Dynamics of film growth of GaAs by MBE from RHEED observation," Appl. Phys. A **31**, 1–8 (1983).
3. M. Kanai, T. Kawai, and S. Kawai, "Atomic layer and unit cell layer growth of (Ca, Sr)CuO_2 thin film by laser molecular beam epitaxy," Appl. Phys. Lett. **58**, 771–773 (1991).
4. G.-Z. Yang, H.-B. Lu, H.-S. Wang, D.-F. Cui, H.-Q. Yang, H. Wang, Y.-L. Zhou, and Z.-H., Chen, "Unit-cell by unit-cell epitaxial growth of $SrTiO_3$ and $BaTiO_3$ thin films by laser molecular beam epitaxy," Chin. Phys. Lett. **14**, 478–480 (1997).
5. D. E. Aspes, J. P. Harbison, A. A. Studna, and L. T. Florez, "Optical-reflectance and electron-diffraction studies of molecular-beam-epitaxy growth transient on GaAs(001)," Phys. Rev. Lett. **59**, 1687–1690 (1987).
6. J. P. Harbison, D. E. Aspnes, A. A. Studna, L. T. Florez, and M. L. Kelly, "Oscillations in the optical response of (001)GaAs and AlGaAs surfaces during crystal growth by molecular beam epitaxy," Appl. Phys. Lett. **52**, 2046–2048 (1988).
7. N. Dietz and K. J. Bachmann, "*p*-polarized reflectance spectroscopy: a highly sensitive real-time monitoring technique to study surface kinetics under steady state epitaxial deposition conditions," Vacuum **47**, 133–140 (1996).
8. K. J. Bachmann, U. Rossow, and N. Dietz, "Real-time monitoring of heteroepitaxial growth processes on the silicon(001) surface by *p*-polarized reflectance spectroscopy," Mater. Sci. Eng., B **35**, 472–378 (1995).
9. J.-T. Zettler, T. Wethkamp, M. Zorn, M. Pristovsek, C. Meyne, K. Ploska, and W. Richter, "Growth oscillations with monolayer periodicity monitored by ellipsometry during metalorganic vapor phase epitaxy of GaAs(001)," Appl. Phys. Lett. **67**, 3783–3785 (1995).
10. X. D. Zhu, H.-B. Lu, G.-Z. Yang, Z.-Y. Li, B.-Y. Gu, and D.-Z. Zhang, "Epitaxial growth of $SrTiO_3$ on $SrTiO_3$(001) using an oblique-incidence reflectance-difference technique," Phys. Rev. B **57**, 2514–2519 (1998).
11. F. Chen, H.-B. Lu, T. Zhao, K.-J. Jin, Z.-H. Chen, and G.-Z. Yang, "Real-time optical monitoring of the heteroepitaxy of oxides by an oblique-incidence reflectance difference technique," Phys. Rev. B **61**, 10,404–10,410 (2000).
12. A. Madhukar, T. C. Lee, M. Y. Yen, P. Chen, J. Y. Kim, S. V. Ghaisas, and P. G. Newman, "Role of surface kinetics and interrupted growth during molecular beam epitaxial growth of normal and inverted GaAs/AlGaAs(100) interfaces: a reflection high-energy electron diffraction intensity dynamics study," Appl. Phys. Lett. **46**, 1148–1150 (1985).
13. X. D. Xiao, Y. L. Xie, and Y. R. Shen, "Surface diffusion probed by linear optical diffraction," Surf. Sci. **271**, 295–298 (1992).
14. X. D. Zhu, Th. Rasing, and Y. R. Shen, "Surface diffusion of CO on Ni(111) studied by diffraction of optical second-harmonic generation off a monolayer grating," Phys. Rev. Lett. **61**, 2883–2885 (1988).
15. D. J. Eaglesham and M. Cerullo, "Dislocation-free Stranski–Krastanow growth of Ge on Si(100)," Phys. Rev. Lett. **64**, 1943–1946 (1990).
16. N. Dietz, D. J. Stephens, and K. J. Bachmann, "*In-situ* multilayer film growth characterization by Brewster angle reflectance differential spectroscopy," in *Diagnostic Techniques for Semiconductor Materials Processing*, O. J. Glembocki, S. W. Pang, F. H. Pollak, G. M. Crean, and G. Larrabee, eds. MRS Symp. Proc. **324**, 27–32 (1994).
17. R. A. Mckee, F. J. Walker, E. D. Specht, G. E. Jellison, Jr., L. A. Boatners, and J. H. Harding, "Interface stability and the growth of optical quality perovskites on MgO," Phys. Rev. Lett. **72**, 2741–2744 (1994).
18. M. Born and E. Wolf, *Principles of Optics*, 6th ed. (Pergamon, Oxford, 1980), pp. 61–66.